PAPER • OPEN ACCESS

Numerical optimization of amplitude-modulated pulses in microwave-driven entanglement generation

View the article online for updates and enhancements.

Quantum Science and Technology

Numerical optimization of amplitude-modulated pulses in microwave-driven entanglement generation

M Duwe[1,2,7] , G Zarantonello[1,2,7,8] , N Pulido-Mateo[1,2] , H Mendpara[1,2] ,
L Krinner[1,2] , A Bautista-Salvador[1,2,3] , N V Vitanov[4] , K Hammerer[5] ,
R F Werner[6] and C Ospelkaus[1,2,3,*]

1   Institut für Quantenoptik, Leibniz Universität Hannover, Welfengarten 1, 30167 Hannover, Germany
2   Physikalisch-Technische Bundesanstalt, Bundesallee 100, 38116 Braunschweig, Germany
3   Laboratorium für Nano- und Quantenengineering, Leibniz Universität Hannover, Schneiderberg 39, 30167 Hannover, Germany
4   Department of Physics, St. Kliment Ohridski University of Sofia, 5 James Bourchier blvd, 1164 Sofia, Bulgaria
5   Institut für Theoretische Physik und Institut für Gravitationsphysik (Albert-Einstein-Institut), Leibniz Universität Hannover,
    Appelstrasse 2, 30167 Hannover, Germany
6   Institut für Theoretische Physik, Leibniz Universität Hannover, Appelstrasse 2, 30167 Hannover, Germany
7   MD and GZ contributed equally to this work.
8   Present address: National Institute of Standards and Technology, Boulder, Colorado 80305, United States of America.
*   Author to whom any correspondence should be addressed.

E-mail: christian.ospelkaus@iqo.uni-hannover.de

Abstract

Microwave control of trapped ions can provide an implementation of high-fidelity two-qubit gates free from errors induced by photon scattering. Furthermore, microwave conductors may be embedded into a scalable trap structure, providing the chip-level integration of control that is desirable for scaling. Recent developments have demonstrated how amplitude modulation of the gate drive can permit a two-qubit entangling operation to become robust against motional mode noise and other experimental imperfections. Here, we discuss a method for the numerical optimization of the microwave pulse envelope to produce gate pulses with noise resilience, considerably faster operation and high energy efficiency.

1. Introduction

Trapped ions are a leading scalable platform for the implementation of quantum algorithms [1–3]. Scaling any hardware will ultimately require the implementation of quantum error correction codes [4, 5] to prevent error propagation in large-scale algorithms. This will require quantum gates with fidelities beyond the fault-tolerance threshold [6, 7]. A universal set of quantum gates requires single-qubit gates and one two-qubit gate capable of entanglement generation [8]. For trapped ions, single-qubit operations have already reached error rates well below 10^{-4} [9, 10]. A major experimental challenge is to obtain similar error rates for a two-qubit entangling gate. Experimental results are approaching the desired gate fidelity [11–14] where large-scale error correction could reasonably be implemented [15, 16]. Unfortunately, two-qubit entangling gates can be affected by a variety of imperfections, the seriousness of which depend on the type of gate itself. Quantum control methods allow to analytically or numerically improve the performance of the gate, providing resilience and robustness against specific error sources. The specifics of the protocol implemented depend on the source of errors addressed for the gate. In the case of noise connected to the qubit frequency, the most straightforward control protocol is the Hahn echo [17], but depending on the gate protocol more advanced schemes can be required. There are multiple protocols which employ pulsed dynamical decoupling [18, 19] and continuous dynamical decoupling [20] or other forms of error suppression [21, 22]. In the case of errors connected to the ion's state of motion, several methods have been studied: Walsh modulation [23], multi-tone fields [24–26], phase modulation [27], frequency modulation [28] and amplitude modulation [29, 30]. The latter has been extensively used in laser-driven operations [29–32], and more recently demonstrated for microwave-driven operations [33].

Hybrid schemes to provide simultaneous insensitivity to motional mode and qubit frequency instabilities have been proposed [34, 35].

Here we present a method to perform numerical optimization of a pulse envelope for amplitude-modulation in Mølmer–Sørensen entangling gates. The method described here allows the phase-space trajectories of the ion motion to be resistant to trap and pulse parameters, like the gate detuning, allowing faster operations while maintaining the same previously demonstrated insensitivity [33]. The optimization itself could be potentially extended to other problems because the technique is rather general. The energy used for the gate is minimized, an important feature in the case of microwave driven operations [36–38], especially in cryogenic environments where cooling power should be limited [39, 40], as excess energy could affect the trapping potential and consequently the ion's motional frequencies.

2. Numerical optimization

The numerical method presented here aims to optimize the amplitude of the bichromatic microwave field which drives the Mølmer–Sørensen entangling gate with the Hamiltonian

$$H = \frac{\hbar}{2}\Omega(t)\sum_{j=1}^{2}(\sigma_j^+ + \sigma_j^-)(a\,e^{i\delta t} + a^\dagger\,e^{-i\delta t}) \tag{1}$$

described in [41–43]. Here $\Omega(t)$ is the Rabi frequency of the microwave pulse.

The gate dynamics can be described by introducing a basic control function $\Omega : [0, \tau] \to \mathbb{R}$. Such functions modulate the motion in phase space of the harmonic oscillator describing the ions' secular motion

$$p(t) = \int_0^t ds\,\sin(\delta s)\Omega(s)$$
$$q(t) = \int_0^t ds\,\cos(\delta s)\Omega(s), \tag{2}$$

where δ is the detuning from the motional mode frequency of the bichromatic drive. At a specific time τ, the gate time, the trajectory described in equation (2) should ideally constitute a loop with an enclosed area A such that $|A| = \pi/2$. In case the trajectory does not return to the initial phase space position or the enclosed area differs from $\pi/2$ the gate fidelity $\mathcal{F}$ will be affected by an error. As a fidelity measure we use the overlap of the generated state with the target Bell state $|\psi\rangle = \frac{1}{\sqrt{2}}(|\uparrow\uparrow\rangle - i|\downarrow\downarrow\rangle)$. Other measures like quantum tomography [44] exist, and should eventually be considered too. The used measure is chosen because it needs less resources [45]. In the future the fidelities could also be measured using a computational approach like randomized benchmarking [46, 47]. In terms of Ω the area is

$$A = \int p\,dq = \int_0^\tau dt\,\cos(\delta t)\Omega(t)\int_0^t ds\,\sin(\delta s)\Omega(s)$$
$$= \frac{1}{2}\int_0^\tau dt\int_0^\tau ds\,\Omega(t)K(t,s)\Omega(s) \tag{3}$$

with the kernel

$$K(t, s) = \cos(\delta\,\max(t, s))\sin(\delta\,\min(t, s)), \tag{4}$$

with $t, s \in [0, \tau]$. Furthermore, as previously stated, it is of interest to minimize the energy dissipated in the trap. Since the gate Rabi rate is proportional to the current flowing in the trap conductors, the energy will be proportional to

$$E = \int_0^\tau dt\,\Omega(t)^2. \tag{5}$$

The optimization done here generates pulses that have a fixed area in phase space while minimizing a cost function, which includes the energy. Since both quantities are given by quadratic expressions, this amounts to finding the pulse Ω which satisfies the generalized eigenvalue equation

$$\hat{A}\Omega = \lambda\hat{E}\Omega \tag{6}$$

with the smallest possible eigenvalue λ [48]. This is because we aim to find the smallest energy for a fixed area, which needs to be $\pi/2$ for the entangling gate interaction. Eigenvectors with a larger eigenvalue therefore have a higher energy. Here $\hat{A}$ and $\hat{E}$ are the operators representing the quadratic expressions A and E. That is $\langle\Omega, \hat{A}\Omega\rangle = A$, so $\hat{A}$ is given by the above kernel $K/2$, and $\hat{E}$ is the identity operator. The

inner product is defined on the Hilbert space $\mathcal{L}^2([0,t], \mathrm{d}t)$. This general form will also apply in the discretized version that we solve numerically, although $\hat{E}$ will then be more complicated. One can use the scheme to achieve additional desirable features, for example, smoothness. To that end we will add to the cost function E a small penalty term with the norm square of the derivative Ω', i.e., use a so-called Sobolev norm [49]. This prevents the derivative of Ω from becoming too large. Moreover, it is easy to include arbitrary linear constraints $\langle \phi, \Omega \rangle = 0$, by solving the generalized eigenvalue problem on a subspace [48]. The most important of these is that the loop closes in phase space, i.e., $p(\tau) = q(\tau) = 0$ in equation (2). We can also ensure that small variations in the detuning δ do not disturb the loop closure, by demanding that the derivatives of $p(\tau)$ and $q(\tau)$ with respect to δ vanish as well. That is we demand Ω to be orthogonal to the following four functions

$$\phi^1 = \cos(\delta t), \qquad \phi^2 = \sin(\delta t)$$
$$\phi^3 = t \, \sin(\delta t), \qquad \phi^4 = t \, \cos(\delta t).$$

ϕ^1 and ϕ^2 ensure that $p(\tau) = q(\tau) = 0$ because

$$\langle \phi^1, \Omega \rangle = \int_0^\tau \mathrm{d}t \, \cos(\delta t) \Omega(t) = 0 \tag{7}$$

and

$$\langle \phi^2, \Omega \rangle = \int_0^\tau \mathrm{d}t \, \sin(\delta t) \Omega(t) = 0. \tag{8}$$

Therefore they ensure a closed loop in phase space but do not increase resilience against mode detunings. The functions ϕ^3 and ϕ^4 are the derivatives of ϕ^1 and ϕ^2 with respect to δ and ensure that small variations in the detuning change the trajectory minimally. Potentially the amount of excluded functions can be increased. One might consider to include even higher derivatives of ϕ^1 and ϕ^2 for more stability with respect to the detuning in higher derivatives. We restricted ourselves to these four functions to not make the subspace too small, which would come at the expense of increased energy. Additional constraints would introduce additional metrics that the numerical method needs to optimize on effectively decreasing the subspace size for each new constraint added. This derivative strategy is reminiscent of the approach used to construct composite pulses [50]. However, here it is used to construct the shape of the pulse rather than the phases of the composite sequence of pulses.

For a numerical analysis, the gate time interval is discretized into $n + 1$ pieces, with cut points $0 =: t_0 < t_1 < t_2 < \cdots < t_n < t_{n+1} := \tau$. Typically $n = 100$, to ensure smoothness between subsequent steps. In the optimization, various functions have to be evaluated at these points. The following basis is used for Ω

$$\chi_k(t) = \begin{cases} \dfrac{t - t_{k-1}}{t_k - t_{k-1}}, & t_{k-1} < t \leqslant t_k \\ \dfrac{t_{k+1} - t}{t_{k+1} - t_k}, & t_k < t \leqslant t_{k+1} \\ 0, & \text{otherwise.} \end{cases} \tag{9}$$

Note that $\chi_k(t_j) = \delta_{kj}$, so the expansion coefficients in

$$\Omega(t) = \sum_{k=1}^n \omega_k \chi_k(t) \tag{10}$$

are exactly the values $\omega_k = \Omega(t_k)$. These coefficients give the gate Rabi rate value at a specific moment t_k. When ϕ^i are the excluded functions, the projection onto their complement is

$$p = \mathbb{1} - \sum_{ij} |\phi^i\rangle G_{ij}^{-1} \langle \phi^j| \,, \tag{11}$$

where $G_{ij} = \langle \phi^i, \phi^j \rangle$ is the corresponding Gram matrix [51], and G^{-1} is its matrix inverse. The energy kernel $\hat{E}_{ij} = \langle \chi_i, \chi_j \rangle$ of equation (5) is adjusted with the Sobolev norm so that

$$\hat{E}_{ij} = \langle \chi_i, \chi_j \rangle + c \cdot \langle \chi_i', \chi_j' \rangle \tag{12}$$

to ensure a soft start, necessary to avoid pseudopotential kicks from parasitic electric fields [52]. This is ensured through the second term, where the parameter c parametrizes the emphasis placed on the 'soft start' condition. In the following we restrict ourselves to the case $c = 1$. This specific choice was made in

Figure 1. Pulse shape and phase space trajectory for $\delta\tau = 6\pi$. The gate time is $\tau = 1000.4\,\mu s$ with a detuning of $\delta/2\pi = 2.998$ kHz. These values are obtained for a specific Rabi frequency of $\Omega_{MS}/2\pi = 1.18$ kHz.

Figure 2. Calculated energy dissipated in the trap for different values of $\delta\tau$. Blue circles correspond to the square gate, green diamonds to the sin² and orange squares to the optimized shapes. The energy dissipated depends on the actual experimental conditions, the values reported here are normalized for comparison.

order to ensure a soft start without increasing the cost function too much. If $c = 0$ then a soft start of the pulse is not guaranteed.

The objective is to minimize the energy E while keeping the area A constant. This can be achieved by solving the generalized eigenvalue problem $\hat{\mathcal{A}}\Omega = \lambda\hat{\mathcal{E}}\Omega$ where $\hat{\mathcal{A}} = p\hat{A}p$ and $\hat{\mathcal{E}} = p\hat{E}p$ are the kernels mentioned above but projected onto the subspace with the projector p defined earlier in equation (11). The eigenvector with the lowest eigenvalue provides the coefficients ω_k that have the best ratio of energy to area. Eigenvectors with larger eigenvalues are therefore not considered. The ratio of δ and τ defines the corresponding eigenvector because the area kernel is dependent on the detuning. Therefore solving the generalized eigenvalue problem for different detunings leads to diverse trajectories. For the Mølmer–Sørensen gate, $\delta\tau = K \cdot 2\pi$, where K is an integer number, needs to hold. The possibility to perform a gate starts with $K = 1$. A possible eigenvector and its phase space trajectory is shown in figure 1 for $\delta\tau = 6\pi$. Instead of performing circles in phase space, as for the square gate, the trajectory starts and ends with narrow loops around the origin. In case of experimental imperfections e.g. in the detuning δ, the resulting (undesired) displacement of the final state from the starting point in phase space is smaller than for the corresponding square-pulse gate. This is the key reason for the robustness of shaped pulses.

Figure 2 shows the energy dissipated in the trap for the square, sin² [33] and the numerically optimized gates. The energy E is calculated with equation (5) for all shapes while maintaining Ω_{MS} constant. For the same value of $\delta\tau$, the optimized pulses dissipate approximately 25% less energy than the square pulses. The main reason for this is the soft start of the pulses, which lowers the integral of $\Omega(t)^2$ over the gate time τ. The largest energy corresponds to the square pulse with $\delta\tau = 36\pi$. All energies in figure 2 are normalized to this value. The numerically optimized gates dissipate more energy than the sin² gates. This is due to the fact that the sinusoidal pulses have an even softer start. The dissipated energy can contribute to gate errors because it may introduce dynamical changes in the mode frequency. Therefore pulses that dissipate less energy are generally preferred to minimize effects such as the mode frequency chirp [53]. On the other hand, pulses with more loops in phase space (higher $\delta\tau$) and thus typically higher energy also feature increased robustness to experimental imperfections (see above). Therefore in our previous work [33] the sin² pulse with $\delta\tau = 36\pi$ was chosen even though it dissipates more energy than lower orders. The numerical optimization could achieve even lower energies if the parameter c, which imposes the 'soft start'
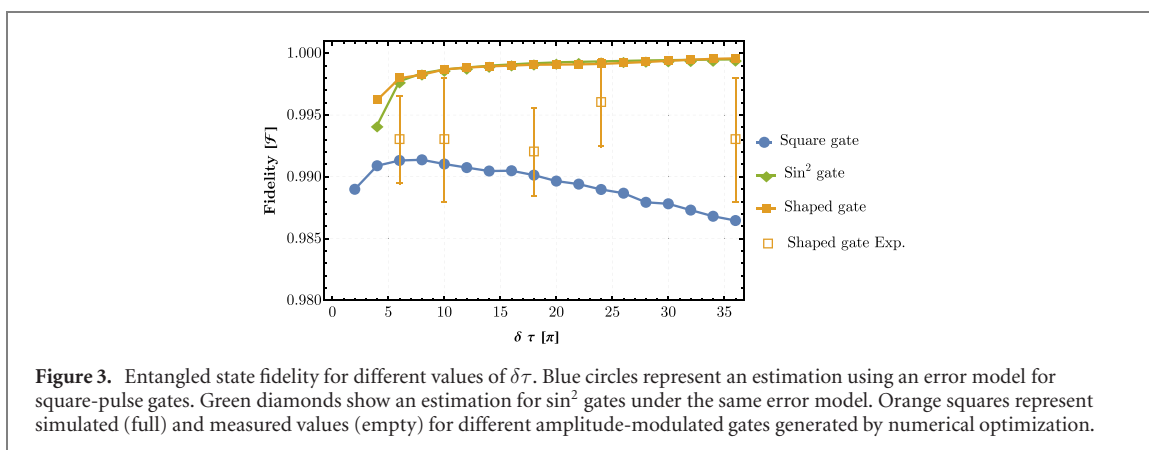
condition, were changed. However, this would come at the cost of a longer gate time τ. Compared to the $\sin^2$ pulses, the optimal pulses identified here require a gate time about 15% shorter for the same value of $\delta\tau$, which is of particular interest for longer sequences in a computational context.

3. Experimental demonstration

The experimental demonstration of the entangling gate pulse envelopes obtained using the method described in section 2 has been done in the setup described in [53, 54]. The experiments have been performed on $^9\text{Be}^+$ ions at a static magnetic field of $|\mathbf{B}_0| = 22.3$ mT, where the chosen qubit transition, $^2\text{S}_{1/2}|F = 2, m_F = 1\rangle \leftrightarrow {}^2\text{S}_{1/2}|F = 1, m_F = 1\rangle$, at $\omega_0 = 2\pi \cdot 1082.55$ MHz is first-order field independent. F and m_F are the quantum numbers for the total angular momentum of the ion and its projection on the quantization axis. The enhanced frequency stability of the qubit transition leads to an increased coherence time of the qubit [55]. Doppler cooling and detection is performed with a 313 nm laser resonant with the $^2\text{S}_{1/2}|F = 2, m_F = 2\rangle \leftrightarrow {}^2\text{P}_{3/2}|m_J = \frac{3}{2}, m_I = \frac{3}{2}\rangle$ transition. Here m_J and m_I represent the projections of the total electronic and nuclear angular momenta onto the quantization axis. For integrated microwave control, three conductors are embedded in the surface-electrode trap: two conductors for driving carrier transitions and one for sideband operations. The latter is designed [56] to produce a strong magnetic field gradient optimized for spin-motional coupling. The microwave amplitude modulation setup is described in [33] and more experimental details can be found in [53]. For implementation purposes, optimized pulse envelopes are produced with $\delta\tau = 6\pi, 10\pi, 18\pi, 24\pi$ and 36π. For a maximum gate Rabi rate of $\Omega_{\text{MS}}/2\pi = 1.18$ kHz, the pulse durations are 1000.4 μs, 1324.8 μs, 1793.77 μs, 2083.4 μs and 2548.7 μs.

    The maximally entangled states generated have been analyzed with a partial tomography procedure [57]. All state populations have been estimated from the global fluorescence emission of the ions by using appropriately placed thresholds in the photon count histograms. Experimental results are reported in figure 3 and compared with the expected theoretical performance of a standard square-pulse gate, the $\sin^2$ pulses and the simulated results of the numerical pulses. π and $\pi/2$ rotations used for state preparation, shelving and analysis are implemented using composite pulses. Specifically, the U5a sequence has been used for π pulses [58] and the five pulse sequence for the $\pi/2$ analysis pulse [50].

    The fidelities for simulated Mølmer–Sørensen gates have been obtained using Qutip [59] simulations and an error model adjusted to reflect the experimental conditions. For the addressed out-of-phase radial motional mode, we considered an average motional state occupation of $\bar{n} = 0.4$, a heating rate of $\dot{\bar{n}} = 8$ s^{-1} and an intrinsic linewidth of $2\pi \times 61$ Hz. A single spectator in-phase mode was included, detuned by $\delta_s/2\pi = 96$ kHz, but considered to be initialized to its motional ground state. Experimentally this mode was effectively Doppler cooled to $\bar{n} = 1$. This approximation was done to allow the simulations to be performed in reasonable time by limiting the amount of simulated Fock states. Evaluation of individual points without this approximation showed no significant variation in the resulting fidelity. The experiments have been performed without a warm-up pulse employed in earlier experiments to minimize dynamical motional mode frequency transients (called 'frequency chirp'), induced by thermal transients in the trap [53]. The absence of this thermalization process before the gate means that the full frequency chirp has to be included in the simulation with a ramp of 0.3 Hz μs^{-1} for up to 1000 μs. For each simulated point, the gate detuning δ has been optimized to yield the highest resulting fidelity. Parameters regarding the imperfection of the microwave pulse shape have been left as in the model of [54]. The decoherence time of our qubit transition has not been considered as it is expected to be much longer than the other experimentally relevant timescales. Dynamical (gate-drive induced) transients of the qubit transition frequency due to AC Zeeman shifts (ACZS) have not been included as an error source in the simulation. One of the reasons behind this choice is that ideally the gate is performed at the same point of null ACZS as for the amplitude-modulated gates. Note that despite this choice, it is expected that fast variations, or non-perfect calibrations, of the ACZS could lead to errors in AM gates. Fast variations of the ACZS can occur due to the ions being displaced from the RF null to reach the null ACZS point. The residual RF field can induce micromotion which in turn will effectively make the ion explore a region of non-null ACZS with both a geometrical and temporal dependence, as discussed in [60]. Further details of the error model are described in [61]. The experimental results shown in figure 3 consistently show infidelities below 1%. The large difference in the fidelity between amplitude-modulated and square-pulse gates at the highest values of $\delta\tau$ demonstrates the resilience of the optimized gates. The infidelities of the $\sin^2$ pulses are of the same order as the newly developed pulses. Therefore the resilience to experimental imperfections is comparable but with faster gate operation.

Figure 3. Entangled state fidelity for different values of $\delta\tau$. Blue circles represent an estimation using an error model for square-pulse gates. Green diamonds show an estimation for $\sin^2$ gates under the same error model. Orange squares represent simulated (full) and measured values (empty) for different amplitude-modulated gates generated by numerical optimization.

4. Conclusions

The numerical method described here provides a framework to design optimized amplitude-modulated gates that are robust with respect to disturbances of the motional mode and possibly obey other desirable constraints. The optimization can be adjusted to include stability to other chosen parameters. In addition, the algorithm minimizes the energy per pulse used to generate a maximally entangled Bell state in microwave driven operations. The experimental verification has been done by implementing multiple optimized pulse envelopes, consistently demonstrating an infidelity of less than 1%. All gates produced with this method were faster than the one described in our previous work [33], which was 2938 μs long. The fastest gate in this work had $\tau \approx 1000$ μs.

In the future, such shaped gates can be integrated with other protocols, such as dynamical decoupling [20], to suppress gate errors connected to the ACZS affecting the qubit frequency during gate operation. The integration of these decoupling protocols would ease the requirements concerning the minimization of the ACZS and provide resilience to small changes of the ACZS [60]. To further increase the gate speed, it is necessary to increase the magnetic field gradient driving the gate. One possibility is given by advanced three-dimensional microwave structures [62]. Given the large errors resulting from the global detection of two-ion fluorescence, more advanced schemes of error characterization are required, possibly in a computational context, such as benchmarking methods [47, 63, 64].

Data availability statement

The data that support the findings of this study are available upon reasonable request from the authors.

ORCID iDs

M Duwe ⬥ https://orcid.org/0000-0001-9767-0112
G Zarantonello ⬥ https://orcid.org/0000-0002-4480-1403
N Pulido-Mateo ⬥ https://orcid.org/0000-0001-5622-7704
H Mendpara ⬥ https://orcid.org/0000-0002-2923-5095
L Krinner ⬥ https://orcid.org/0000-0001-7626-2574
A Bautista-Salvador ⬥ https://orcid.org/0000-0002-6528-0117
N V Vitanov ⬥ https://orcid.org/0000-0002-8599-4766
K Hammerer ⬥ https://orcid.org/0000-0002-7179-0666
R F Werner ⬥ https://orcid.org/0000-0003-2288-468X
C Ospelkaus ⬥ https://orcid.org/0000-0002-4170-2936

References

[1] Bermudez A *et al* 2017 *Phys. Rev.* X **7** 041061
[2] Bruzewicz C D, Chiaverini J, McConnell R and Sage J M 2019 *Appl. Phys. Rev.* **6** 021314
[3] Pino J M *et al* 2021 *Nature* **592** 209–13
[4] Steane A M 1996 *Phys. Rev. Lett.* **77** 793–7
[5] Knill E 2005 *Nature* **434** 39–44
[6] Preskill J 1998 *Proc. R. Soc.* A **454** 385–410
[7] Knill E 2010 *Nature* **463** 441–3
[8] DiVincenzo D P 1995 *Phys. Rev.* A **51** 1015–22
[9] Brown K R, Wilson A C, Colombe Y, Ospelkaus C, Meier A M, Knill E, Leibfried D and Wineland D J 2011 *Phys. Rev.* A **84** 030303
[10] Harty T P, Allcock D T C, Ballance C J, Guidoni L, Janacek H A, Linke N M, Stacey D N and Lucas D M 2014 *Phys. Rev. Lett.* **113** 220501
[11] Ballance C, Harty T, Linke N, Sepiol M and Lucas D 2016 *Phys. Rev. Lett.* **117** 060504
[12] Gaebler J *et al* 2016 *Phys. Rev. Lett.* **117** 060505
[13] Srinivas R *et al* 2021 *Nature* **597** 209–13
[14] Clark C R *et al* 2021 *Phys. Rev. Lett.* **127** 130505
[15] Ryan-Anderson C *et al* 2021 arXiv:2107.07505 [quant-ph]
[16] Hilder J *et al* 2021 arXiv:2107.06368 [quant-ph]
[17] Hahn E L 1950 *Phys. Rev.* **80** 580–94
[18] Manovitz T, Rotem A, Shaniv R, Cohen I, Shapira Y, Akerman N, Retzker A and Ozeri R 2017 *Phys. Rev. Lett.* **119** 220505
[19] Arrazola I, Casanova J, Pedernales J S, Wang Z Y, Solano E and Plenio M B 2018 *Phys. Rev.* A **97** 052312
[20] Bermudez A, Schmidt P O, Plenio M B and Retzker A 2012 *Phys. Rev.* A **85** 040302
[21] Ivanov S S and Vitanov N V 2015 *Phys. Rev.* A **92** 022333
[22] Arrazola I, Plenio M, Solano E and Casanova J 2020 *Phys. Rev. Appl.* **13** 024068
[23] Hayes D, Clark S M, Debnath S, Hucul D, Inlek I V, Lee K W, Quraishi Q and Monroe C 2012 *Phys. Rev. Lett.* **109** 020503
[24] Haddadfarshi F and Mintert F 2016 *New J. Phys.* **18** 123007
[25] Shapira Y, Shaniv R, Manovitz T, Akerman N and Ozeri R 2018 *Phys. Rev. Lett.* **121** 180502
[26] Webb A E, Webster S C, Collingbourne S, Bretaud D, Lawrence A M, Weidt S, Mintert F and Hensinger W K 2018 *Phys. Rev. Lett.* **121** 180501
[27] Milne A R, Edmunds C L, Hempel C, Frey V, Mavadia S and Biercuk M J 2018 arXiv:1808.10462 [quant-ph]
[28] Leung P H and Brown K R 2018 *Phys. Rev.* A **98** 032318
[29] Zhu S L, Monroe C and Duan L M 2006 *Phys. Rev. Lett.* **97** 050505
[30] Roos C F 2008 *New J. Phys.* **10** 013002
[31] Schäfer V M, Ballance C J, Thirumalai K, Stephenson L J, Ballance T G, Steane A M and Lucas D M 2018 *Nature* **555** 75–8
[32] Figgatt C, Ostrander A, Linke N M, Landsman K A, Zhu D, Maslov D and Monroe C 2019 *Nature* **572** 368
[33] Zarantonello G, Hahn H, Morgner J, Schulte M, Bautista-Salvador A, Werner R F, Hammerer K and Ospelkaus C 2019 *Phys. Rev. Lett.* **123** 260503
[34] Lishman J and Mintert F 2020 *Phys. Rev. Res.* **2** 033117
[35] Sutherland R T *et al* 2020 *Phys. Rev.* A **101** 042334
[36] Mintert F and Wunderlich C 2001 *Phys. Rev. Lett.* **87** 257904
[37] Ospelkaus C, Langer C E, Amini J M, Brown K R, Leibfried D and Wineland D J 2008 *Phys. Rev. Lett.* **101** 090502
[38] Sutherland R T, Srinivas R, Burd S C, Leibfried D, Wilson A C, Wineland D J, Allcock D T C, Slichter D H and Libby S B 2019 *New J. Phys.* **21** 033033
[39] Srinivas R 2020 Laser-free trapped-ion quantum logic with a radiofrequency magnetic field gradient *PhD Thesis* University of Colorado Boulder
[40] Dubielzig T 2021 Ultra-low vibration closed-cycle cryogenic surface-electrode ion trap apparatus *PhD Thesis* Gottfried Wilhelm Leibniz Universität Hannover
[41] Mølmer K and Sørensen A 1999 *Phys. Rev. Lett.* **82** 1835
[42] Solano E, de Matos Filho R L and Zagury N 1999 *Phys. Rev.* A **59** R2539
[43] Milburn G J, Schneider S and James D F V 2000 *Fortschr. Phys.* **48** 801–10
[44] White A G, Gilchrist A, Pryde G J, O'Brien J L, Bremner M J and Langford N K 2007 *J. Opt. Soc. Am.* B **24** 172
[45] da Silva M P, Landon-Cardinal O and Poulin D 2011 *Phys. Rev. Lett.* **107** 210404
[46] Knill E *et al* 2008 *Phys. Rev.* A **77** 012307
[47] Gaebler J P *et al* 2012 *Phys. Rev. Lett.* **108** 260503
[48] Ghojogh B, Karray F and Crowley M 2019 arXiv:1903.11240 [cs, stat]
[49] Alt H W 2016 *Linear Functional Analysis* (Berlin: Springer)
[50] Torosov B T and Vitanov N V 2011 *Phys. Rev.* A **83** 053420
[51] Petersen P 2012 *Linear Algebra* (*Undergraduate Texts in Mathematics*) (Berlin: Springer)
[52] Warring U, Ospelkaus C, Colombe Y, Brown K R, Amini J M, Carsjens, Leibfried D and Wineland D J 2013 *Phys. Rev.* A **87** 013437
[53] Hahn H, Zarantonello G, Schulte M, Bautista-Salvador A, Hammerer K and Ospelkaus C 2019 *npj Quantum Inf.* **5** 70
[54] Hahn H 2019 Two-qubit microwave quantum logic gate with ^{9}Be$^+$ ions in scalable surface-electrode ion traps *PhD Thesis* Gottfried Wilhelm Leibniz Universität Hannover
[55] Langer C *et al* 2005 *Phys. Rev. Lett.* **95** 060502
[56] Carsjens M, Kohnen M, Dubielzig T and Ospelkaus C 2014 *Appl. Phys.* B **114** 243–50
[57] Sackett C A *et al* 2000 *Nature* **404** 256–9
[58] Genov G T, Schraft D, Halfmann T and Vitanov N V 2014 *Phys. Rev. Lett.* **113** 043001
[59] Johansson J R, Nation P D and Nori F 2013 *Comput. Phys. Commun.* **184** 1234–40
[60] Zarantonello G 2020 Robust high fidelity microwave near-field entangling quantum logic gate *PhD Thesis* Gottfried Wilhelm Leibniz Universität Hannover

[61] Schulte M 2020 Entanglement in Ramsey interferometry, optical atomic clocks and trapped ions *PhD Thesis* Gottfried Wilhelm Leibniz Universität Hannover

[62] Hahn H, Zarantonello G, Bautista-Salvador A, Wahnschaffe M, Kohnen M, Schoebel J, Schmidt P O and Ospelkaus C 2019 *Appl. Phys.* B **125** 154

[63] Erhard A *et al* 2019 *Nat. Commun.* **10** 5347

[64] Baldwin C H, Bjork B J, Gaebler J P, Hayes D and Stack D 2020 *Phys. Rev. Res.* **2** 013317